Supplementary Material for "Extracting the Lifetime of a Synthetic Two-Level System"

Gabriel Margiani,[1] Sebastián Guerrero,[1] Toni L. Heugel,[2] Christian Marty,[1] Raphael Pachlatko,[1] Thomas Gisler,[1] Gabrielle D. Vukasin,[3] Hyun-Keun Kwon,[3] James ML. Miller,[3] Nicholas E. Bousse,[3] Thomas W. Kenny,[3] Oded Zilberberg,[4] Deividas Sabonis,[1] and Alexander Eichler[1]

[1] *Laboratory for Solid State Physics, ETH Zürich, CH-8093 Zürich, Switzerland.*
[2] *Institute for Theoretical Physics, ETH Zürich, CH-8093 Zürich, Switzerland.*
[3] *Departments of Mechanical and Electrical Engineering, Stanford University, Stanford, California 94305, USA*
[4] *Department of Physics, University of Konstanz, D-78457 Konstanz, Germany.*

PROBABILITY DENSITY

In this section, we briefly detail our analysis steps yielding the probability density shown in Fig. 2(c) in the main text. First, we find the deterministic equations of motion for the "slow" quadrature amplitudes u and v. To this end, we use the so-called van der Pol transformation and lowest-order Krylov–Bogoliubov averaging method [1–3], to replace the full time-dependent equation of motion [cf. Eq. (1) in the main text] by time-independent averaged equations of motion. The white noise term ξ is transformed in a similar way using the method described in [4, 5] which yields

$$\begin{aligned}\dot{u} &= -\frac{\gamma u}{2} - \left(\frac{3\alpha}{8\omega_d}X^2 + \frac{\omega_0^2-\omega_d^2}{2\omega_d} + \frac{\lambda\omega_0^2}{4\omega_d}\right)v + \frac{1}{\sqrt{2}\omega_0}\Xi_u\,,\\ \dot{v} &= -\frac{\gamma v}{2} + \left(\frac{3\alpha}{8\omega_d}X^2 + \frac{\omega_0^2-\omega_d^2}{2\omega_d} - \frac{\lambda\omega_0^2}{4\omega_d}\right)u + \frac{1}{\sqrt{2}\omega_0}\Xi_v\,,\end{aligned} \tag{S1}$$

where $\omega_d = 2\pi f_d$ is the angular demodulation frequency and $X^2 = u^2 + v^2$. Ξ_u and Ξ_v are new independent white noise processes of strength σ. Equations (S1) provide a good description of the system when λ, γ/ω_0, $(\alpha/\omega_0^2)x^2$, and $\alpha\sigma^2/\omega_0^2$ are small.

We use the stochastic differential equations (S1) to derive the corresponding Fokker-Planck equation [6, 7] that describes the time evolution of the probability density $p(u,v,t)$:

$$\begin{aligned}\partial_t p(u,v,t) = -\partial_u\Bigg\{\frac{1}{2\omega_d}\left[\gamma\omega_d u + \left(\alpha\frac{3}{4}X^2 + (\omega_0^2-\omega_d^2) + \frac{\lambda}{2}\omega_0^2\right)v\right]p\Bigg]\\ - \partial_v\left[\frac{1}{2\omega_d}\left(\gamma\omega_d v + \left(-\alpha\frac{3}{4}X^2 - (\omega_0^2-\omega_d^2) + \frac{\lambda}{2}\omega_0^2\right)u\right]p\right\} + \frac{1}{2}\left(\frac{\sigma}{\sqrt{2}\omega_d}\right)^2(\partial_u^2+\partial_v^2)p\,.\end{aligned} \tag{S2}$$

We then solve this partial differential equation (PDE) numerically for the steady state ($\dot{p}=0$) which is reached after long times and plot the outcome for the experimental parameters in Fig. 2(c).

ALLAN VARIANCE FOR A SYSTEM DOMINATED BY TELEGRAPH NOISE

In this section, we provide a short derivation of the Allan variance of a system subject to telegraph noise [cf. Eq. (5) in the main text]. The Allan variance can be calculated via the autocorrelation function. For a random telegraph signal x which switches between B and $-B$ the autocorrelation function is given by [8]:

$$\langle x(t)x(t+\tau_A)\rangle = B^2 e^{-2\tau_A/\tau}\,, \tag{S3}$$

where $1/\tau$ is the mean rate of transitions. The Allan variance is obtained by the following expectation value for

the cumulative amplitudes $y(t) = \int_0^t x(t')dt'$

$$\begin{aligned}
\sigma_A^2(\tau_A) &= \frac{1}{2\tau_A^2}\langle (y(t+2\tau_A) - 2y(t+\tau_A) + y(t))^2 \rangle \\
&\underbrace{=}_{\text{plug-in definition of y}} \frac{1}{2\tau_A^2}\left\langle \left(\int_0^{t+2\tau} x(t')dt' - 2\int_0^{t+\tau_A} x(t')dt' + \int_0^t x(t')dt' \right)^2 \right\rangle \\
&\underbrace{=}_{\text{cancel terms in parenthesis}} \frac{1}{2\tau_A^2}\left\langle \left(-\int_t^{t+\tau_A} x(t')dt' + \int_{t+\tau_A}^{t+2\tau_A} x(t')dt' \right)^2 \right\rangle \\
&\underbrace{=}_{\text{expand the square}} \frac{1}{2\tau_A^2}\left\langle 2\int_0^t \int_0^t x(t')x(t'')dt''dt' - 2\int_0^t \int_0^t x(t'+\tau_A)x(t'')dt''dt' \right\rangle \\
&\underbrace{=}_{\text{apply Eq. S3}} \frac{0.8}{2\tau_A^2} 2B^2 \int_0^{\tau_A} \int_0^{\tau_A} e^{-2|t'-t''|/\tau} - e^{-2(t'-t''+\tau_A)/\tau} dt''dt' \\
&\underbrace{=}_{\text{evaluate the integral}} -B^2 \frac{-4\tau_A/\tau + e^{-4\tau_A/\tau} - 4e^{-2\tau_A/\tau} + 3}{4\tau_A^2/\tau^2}.
\end{aligned} \tag{S4}$$

We can now look for the maximum of the obtained expression by setting the first derivative equal to 0, i.e. $d\sigma_A^2/d\tau_A \equiv 0$. Expanding the numerator in τ_A around τ up to forth order, we find that the maximum is located at $\tau_A \approx 0.946\tau \approx \tau$.

INVESTIGATION OF CIRCLE THRESHOLD RADIUS

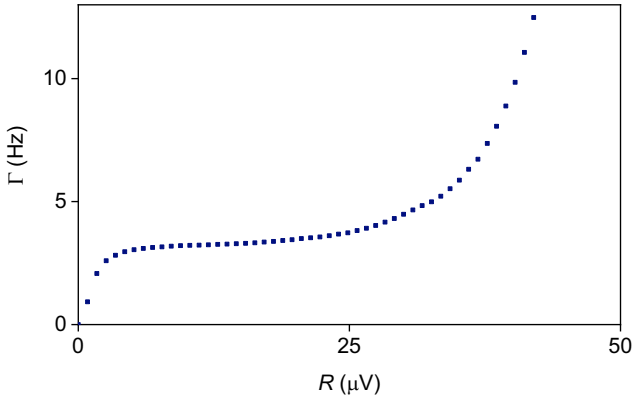

FIG. S1: **Parametron switching rate dependence on the radius of the threshold circle.**

CALCULATION OF POWER SPECTRAL DENSITY AND AUTOCORRELATION

The data was recorded as two quadratures u and v that result from the signal demodulation at half the parametric drive frequency. The quadratures were then digitized at a sampling rate of 899.46 Sa/s. The total length of the time trace was 899.94 s with a total number of 809472 recorded points. The two quadratures were then transformed into the spectral domain by using the complex (u+iv) Welch power spectral density function in Python. Afterwards, the resulting double-sided power spectral density was converted to a single sided power spectral density. As a last step, Eq. 2 in the main text was fitted to the data.

The autocorrelation $AC(T)$ for correlation times $T = n\delta t$ where n is an integer and δt is the sampling time, is calculated from the measured quadrature data points u_k and v_k in the following way. Let $a_k = u_k + iv_k$ be the complex data points, then $M_i^j = \frac{1}{j-i+1}\sum_{k=i}^{j} a_k$ is the mean of a_k for $i \leq k \leq j$, and $\sigma_i^j = \sqrt{\frac{1}{j-i+1}\sum_{k=i}^{j}(a_k - M_i^j)\overline{(a_k - M_i^j)}}$

is the standard deviation, where N the total number of data points. Here $\overline{(C)}$ denotes the complex conjugate and $\mathrm{Re}(C)$ the real part of a complex value C. The autocorrelation is then:

$$AC(T = n\delta t) = \mathrm{Re}\left(\frac{1}{N-n}\frac{1}{\sigma_1^{N-n}\sigma_{n+1}^{N}}\sum_{i=1}^{N-n}(a_i - M_1^{N-n})\overline{(a_{i+n} - M_{n+1}^{N})}\right) \tag{S5}$$

We fit Eq. (S3) to the resulting $AC(T)$ to extract the switching rate $\Gamma = 1/\tau$.

SWITCHING RATE AS A FUNCTION OF σ_V

Below, we show the switching rate that was estimated with all methods as a function of noise strength in a range where a two-level system exists. The parametric drive strength for this set was chosen to be $V_{in} = 0.436$ V measured on resonance at $f = 0.438$ MHz.

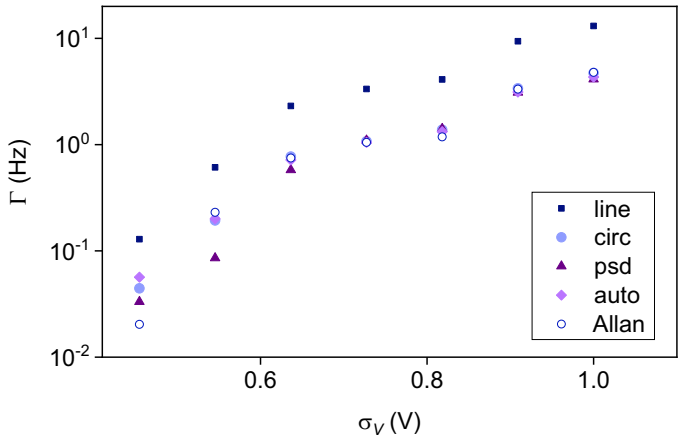

FIG. S2: **Comparison of results for Γ obtained with different rate estimation methods.** Switching rate as a function of noise amplitude σ_V for $\Delta = 0$ and $V_{\mathrm{in}} = 0.436$ V estimated using simple average-based threshold (blue square), circle-based threshold (circles), power spectral density of telegraph noise (triangle), autocorrelation (star) and Allan deviation (hollow circle). Note that for low values of noise (roughly $\sigma_V < 0.6$ V) the larger discrepancies between the four rate estimation methods (circle-based, PSD, autocorrelation and Allan deviation) appear due to a small switching rate (small number of switching events).

We next comment on small deviations between switching rates estimated using different methods in the Fig. S2. In the parametron, we have two attractors in a rotating two-dimensional phase-space. One can think of the situation to be similar to a double-well potential well along one phase-space axis, alongside a single confining well along the perpendicular axis. As such, the system exhibits "fast" oscillations in the basins of phase-space as well as "slower switching" event where a phase-slip occurs and the oscillator moves from one phase state to the other. This is the reason behind the fact that the noise exhibits more involved dynamics than in a 1D double-well potential.

Our study here focuses on comparing methods by which to extract the different fluctuation sources, and specifically estimate the slow activation dynamics. To this end, we use the phenomenological observation that the activation rates are slower than those around the attractor, and evaluate the PSD, auto-correlation, and Allan-variance based on the assumption of having solely telegraph noise. We search for clear signatures of the slow dynamics, where we can differentiate them from the fast ones.

COUPLING OF MULTIPLE MICROMECHANICAL RESONATORS

Resonator networks for advanced applications could be realized through bilinear, resonant coupling of several KPOs [9, 10]. For micromechanical resonators such as those studied here, bilinear coupling can be achieved in multiple ways, the most common being: pairwise (I) capacitive (II) inductive, (III) optical or, (IV) mechanical coupling, or (V) indirect all-to-all coupling through a separate radio-frequency cavity. Commonly, in the design of networks, the

most complex task will be the design of multiple connections with tunable interaction strength. The following classes of coupling architectures can be envisaged:

Proximity coupling. Exchange of photons/phonons between resonators leads to nearest-neighbor coupling. For mechanical resonators, vibrations transmitted evanescently through the substrate or electrostatic interactions through the vacuum are sources of proximity coupling. The coupling can be set via geometric design but generally not tuned in the finished device.

Connector lines. Electrical striplines or optical waveguides that are proximity coupled to two separate resonators can act as a relay to achieve coupling between distant devices. An added advantage is that variable coupling can be obtained through changes in the transmission coefficient of the line. For instance, electrical connector lines can contain an inductive element or a tunable resonator whose transmission can be tuned.

The *Lechner-Hauke-Zoller (LHZ) model.* All-to-all coupling between more than two or three devices poses a severe challenge due to the necessity of a complex network of connector lines. In the *minor embedding scheme* [11, 12], this problem is partially mitigated by creating chains of strongly coupled KPOs that are weakly coupled to other chains, where each chain effectively corresponds to a single logic unit. The LHZ model, on the other hand, presents a more radical possibility to build an all-to-all network using individually adjustable couplings, but without the complexity of a physical connector network [13, 14]. In the LHZ model, the pairwise orientation of network states is encoded in additional parametron devices, and there is no need for physical all-to-all connections.

Nondegenerate resonators with parametric coupling. Many implementations of KPOs rely on degenerate parametric devices, i.e., they all have nominally identical resonance frequencies $\omega_i = \omega_j = \omega_0$ and driving frequencies at $2\omega_0$. In general, nondegenerate resonators have negligible coupling. However, three-wave mixing [15, 16] offers a method for sizable and tunable coupling between nondegenerate parametrons; devices with different resonance ($\omega_i \neq \omega_j$ for all pairs) and driving frequencies ($2\omega_i$, $2\omega_j$, etc.) are coupled to each other through a common medium, for instance a low-Q optical cavity [17] that is proximity-coupled to all resonators. Modulating the cavity field at the frequency differences ($\omega_i - \omega_j$) generates parametric frequency up- and down-conversion between device pairs [18, 19]. The parametrons are thus in effect resonantly coupled.

[1] N. M. Krylov and N. N. Bogoliubov, *Introduction to Non-Linear Mechanics.(AM-11), Volume 11* (Princeton University Press, 1947).
[2] L. Papariello, O. Zilberberg, A. Eichler, and R. Chitra, Phys. Rev. E **94**, 022201 (2016).
[3] J. Guckenheimer and P. Holmes, *Nonlinear oscillations, dynamical systems, and bifurcations of vector fields*, Applied mathematical sciences (Springer-Verlag, 1990).
[4] R. Z. Khas'minskii, Theory of Probability & Its Applications **11**, 390 (1966).
[5] International Journal of Non-Linear Mechanics **21**, 111 (1986), ISSN 0020-7462.
[6] H. Risken, *The Fokker-Planck Equation* (Springer Berlin Heidelberg, 1996).
[7] T. D. Frank, *Nonlinear Fokker-Planck Equations* (Springer Berlin Heidelberg, 2005).
[8] Y. Yamamoto, *Lecture notes: Fundamentals of noise processes*, uRL: https://www.nii.ac.jp/qis/first-quantum/e/forStudents/lecture/index.html.
[9] L. Bello, M. Calvanese Strinati, E. G. Dalla Torre, and A. Pe'er, Phys. Rev. Lett. **123**, 083901 (2019), URL https://link.aps.org/doi/10.1103/PhysRevLett.123.083901.
[10] T. L. Heugel, O. Zilberberg, C. Marty, R. Chitra, and A. Eichler, arXiv preprint arXiv:2103.02625 (2021).
[11] V. Choi, Quantum Information Processing **7**, 193 (2008).
[12] V. Choi, Quantum Information Processing **10**, 343 (2011).
[13] W. Lechner, P. Hauke, and P. Zoller, Science Advances **1** (2015).
[14] S. Puri, C. K. Andersen, A. L. Grimsmo, and A. Blais, Nature Communications **8**, 15785 (2017).
[15] B. Abdo, A. Kamal, and M. Devoret, Phys. Rev. B **87**, 014508 (2013).
[16] Y. Y. Gao, B. J. Lester, Y. Zhang, C. Wang, S. Rosenblum, L. Frunzio, L. Jiang, S. Girvin, and R. J. Schoelkopf, Phys. Rev. X **8**, 021073 (2018).
[17] A. Grimm, N. E. Frattini, S. Puri, S. O. Mundhada, S. Touzard, M. Mirrahimi, S. M. Girvin, S. Shankar, and M. H. Devoret, Nature **584**, 205 (2019).
[18] J. Tucker and D. F. Walls, Annals of Physics **52**, 1 (1969).
[19] A. C. Turner, M. A. Foster, A. L. Gaeta, and M. Lipson, Optics express **16**, 4881 (2008).